Senior Honours Project
The Physics of Morphologically Diverse Bacteria in Moving Fluids

Emma Allen
29th November 2024

Abstract

Large systems of so called banana-shaped particles suspended in a fluid provide an effective model for understanding the role of bacterial motion in sludge bulking seen in wastewater treatment. To analyse this system, it is useful to first understand the dynamics of a single bacterium. By modelling this bacterium as a banana-shaped polymer and employing Molecular Dynamics in Multi-Particle Collision Dynamics, the rotational dynamics are studied as its curvature angle is varied from 0 to 2π. The particle is suspended in a fluid with a constant shear flow, confined within a two-dimensional box with periodic boundary conditions applied to the vertical walls. It is found that the particle follows a Jeffery's Orbit trajectory. However, diffusive rotation (noise) is found to have a significantly greater influence on the rotational dynamics than the curvature angle, as indicated by the Péclet number, which is calculated to be 12.91 ± 0.59. These effects cause noticeable deviations from theoretical predictions and highlight it is critical to account for noise in computational models for bacterial motion in wastewater.

Declaration

I declare that this project and report is my own work.

Signature: *EmmaAllen*   Date: 29/11/2024

Supervisors: Dr. Tyler N Shendruk and Dr. Gavin Melaugh   10 Weeks

Contents

1   Introduction

Bacteria are one of the most abundant organisms on Earth, inhabiting almost every environment. By considering their motion, they can be divided into two categories: motile bacteria, which are capable of self-propulsion, often using structures like flagella, and non-motile bacteria, which lack such mechanisms and move passively through external influences such as fluid shear or diffusion [1]. A common non-motile bacterium is *Microthrix parvicella* [2] which is one bacterium responsible for sludge bulking in wastewater treatment plants. Sludge bulking is where sludge fails to separate out in a sedimentation tank, causing blockages in the waste water system [3]. Bulking can be seen as a microbiological problem due to the occurrence of a specific species of bacteria [4] or as a physics problem due to the growth and movement of bacteria with a filamentous morphology [5], the bacteria may accumulate and become compacted. This aggregation can result in a blockage caused by the jamming of the bacteria.

Focusing on the latter leads us to consider systems of fluid with particles suspended throughout, a colloidal system. By modelling the bacteria as rods one is able to understand their expected trajectories and consider additional factors that could contribute to sludge bulking. One potential factor is if the bacteria had a curved morphology as oppose to a straight rod. Since multiple bacteria, including *Microthrix parvicella*, exhibit curved morphologies, studying this property is highly useful. This can be explored through simulations of so called 'banana-shaped colloids' [6], hereafter termed bananas.

Understanding this system depends on understanding the behaviour of large numbers of these bananas. To achieve this, it is essential to first study how an individual banana behaves when suspended in a fluid. This acts as the prime motivation for this project. By understanding the rotational dynamics of a single banana, one can establish a foundation for modelling large quantities of bananas in a fluid, which in turn could be used to explore the implications in sludge bulking.

In this project, bananas are modelled as analogs for bacteria with curved morphologies to investigate their behaviour under in a fluid with constant shear rate. By employing Molecular Dynamics in Multi-Particle Collision Dynamics (MD in MPCD) the motion of bananas is simulated to explore how bacterial shape influences their rotation. The project commences by providing a theoretical background on particle dynamics in this setup, followed by an explanation of the simulation setup and an analysis of the results for five different bananas with curvatures of $0, \frac{\pi}{2}, \pi, \frac{3\pi}{2}$ and 2π radians.

2   Background

2.1   Fluid Flow

Before explaining the bananas, one first needs a fluid in which they will be suspended. In order to describe this fluid, we begin with the Navier Stokes equations [7], which describes the motion of various fluids. Primarily we are concerned with the following

$$\frac{\partial \mathbf{u}}{\partial t} + (\mathbf{u} \cdot \nabla)\mathbf{u} = -\frac{1}{\rho}\nabla p + \nu \nabla^2 \mathbf{u} + \mathbf{f}. \tag{1}$$

$$\frac{\partial \rho}{\partial t} + \nabla \cdot (\rho \mathbf{v}) = 0 \tag{2}$$

Firstly looking at equation 1, the term $\frac{\partial \mathbf{u}}{\partial t}$ represents the local acceleration, which is the rate of change of the fluid's velocity at a point with respect to time. The term $(\mathbf{u} \cdot \nabla)\mathbf{u}$ is the convective acceleration or advection term, which represents the change in velocity due to the motion of the fluid itself. The term $-\frac{1}{\rho}\nabla p$ is the pressure gradient term, which accounts for the force exerted by the pressure difference in the fluid, where p is the pressure and ρ is the fluid density. The term $\nu \nabla^2 \mathbf{u}$ is the viscous term, with ν being the kinematic viscosity, and it represents the diffusion of momentum in the fluid due to viscosity. Finally, $\mathbf{f}$ represents the external forces acting on the fluid, such as gravity. In essence this is a statement of momentum conservation. Moving on to equation 2, commonly called the continuity equation. This equation arises from the principle that the rate of mass entering a region must equal the rate of mass leaving that region. With the pre-defined meanings of ρ (fluid density) and $\mathbf{v}$ (velocity field), the continuity equation serves as a mathematical statement of mass conservation [7].

These equations have numerous applications, boundary conditions, and solution methods. However, this project solely focuses on the flow of a viscous fluid between two parallel plates in two dimensions with no external forces, allowing for certain simplifications. This type of flow is characterised by a linear velocity profile, commonly referred to as Couette flow [8]. This velocity profile can be established by keeping one surface stationary while moving the other, or by moving both walls with equal magnitude in opposite directions (figure 1). Equal but opposite moving walls is selected for simplicity in simulations that are performed.
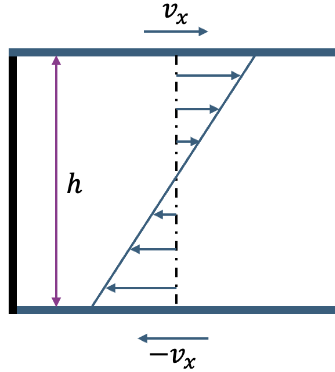

Figure 1: Illustration of the setup used throughout the project. A two dimensional square box with height, h. The horizontal walls move with the same speed, v_x but in opposite directions, giving rise to Couette flow.

To calculate the shear rate, we make a number of assumptions. First, it is assumed that the only non-zero velocity component is in the x-direction, aligned with the flow.

Additionally, the velocity and pressure are considered time-independent, and no external forces are acting on the system. Starting with the continuity equation, with these assumptions, it simplifies to

$$\frac{\partial u_x(y)}{\partial x} = 0. \tag{3}$$

Now the planar Navier Stokes equations for incompressible fluid with uniform, constant viscosity become [9]

$$\frac{\partial p}{\partial x} = \mu \frac{\partial^2 u_x(y)}{\partial^2 y}, \tag{4}$$

$$\frac{\partial p(x)}{\partial y} = 0, \tag{5}$$

As pressure is only a function of x, equation 4 can be integrated to find

$$u_x = \frac{1}{\mu}\frac{dp}{dx}\frac{y^2}{2} + C_1 y + C_2, \tag{6}$$

where C_1 and C_2 are integration constants. These constants are determined by applying no-slip boundary conditions on the upper and lower plates. Physically this condition means that the layer of fluid directly next to the plate has a velocity of zero relative to the plate [10]. Mathematically, these boundary conditions are expressed as

$$u_x(h) = v_x \quad \text{and} \quad u_x(0) = -v_x, \tag{7}$$

$$C_1 = \frac{v_x}{h} - \frac{C_2}{h} \quad \text{and} \quad C_2 = -v_x. \tag{8}$$

Which yields the solution

$$u_x = \frac{2v_x y}{h}. \tag{9}$$

Having determined the velocity of the fluid, one can find the shear rate, $\dot{\gamma}$; a measure of how quickly the velocity of a fluid layer changes with respect to the distance from a reference layer [11]. In general, it is defined as

$$\dot{\gamma} = \frac{du(y)}{dy}, \tag{10}$$

where $u(y)$ is the velocity of the field and y is the perpendicular distance from the plane. For the setup demonstrated in figure 1, the shear rate becomes

$$\dot{\gamma} = \frac{du}{dy} = \frac{d}{dy}\left(\frac{2v_x}{h}y\right) = \frac{2v_x}{h}. \tag{11}$$

This completes the description of the velocity profile and shear rate for Couette flow which the bananas will be suspended in. Now we seek to understand the forces acting on the suspended banana in this fluid. In particular, we are interested in how the balance between rotational diffusion and vorticity influences the rotational motion of the bananas, which is characterised by the Péclet number.

2.2 Péclet Number

When suspended in a fluid, there are two modes that will make bananas rotate, these are rotational diffusion and vorticity.

Rotational diffusion is driven by Brownian motion [12], which results from thermal fluctuations in the fluid. In this process, small fluid particles collide with the banana, causing random changes in its orientation. Although these random collisions are unlikely to result in full rotations, they lead to small, unpredictable fluctuations in the banana's orientation. This type of motion is visualised as random fluctuations in the banana's orientation. In simulations, it is referred to as noise.

On the other hand, vorticity is a measure of local rotation or the tendency of fluid elements to spin in a shear flow [13]. In contrast to the random nature of rotational diffusion, vorticity generates a more organised rotational motion of the banana, where the fluid's shear flow induces a continuous, structured rotation. Visually one would see the banana completing full rotations in fluid.

To quantify which of these two modes, rotational diffusion or vorticity dominates the banana's rotational motion, we use the Péclet number [14]. This dimensionless number can be calculated in different ways depending on the system; in our case for rotational motion, it is defined as

$$\text{Pe} = \frac{\text{Vorticity}}{\text{Diffusion}}. \tag{12}$$

Vorticity is dominant when the Péclet number is greater than one, whereas diffusion is dominant if the Péclet number is less than one. If it is equal to one, the flow is equally dominated by both vorticity and diffusion. It is important to note, even with a Péclet number greater than one diffusion is still present. The range of the Péclet number spans several orders of magnitude, thus it is generally compared in terms of orders of magnitude rather than precise numerical values.

In order to calculate the Péclet number, both the vorticity and diffusion transport must be quantified. For our purposes, vorticity can be simply quantified by the shear rate, $\dot{\gamma}$ [15]. This is valid because we have a simple shear as described in section 2.1.

Meanwhile, diffusion is given by the rotational diffusion coefficient D_R. To calculate D_R, the Mean Square Angular Displacement (MSAD) is calculated [16]. The MSAD quantifies the spread of a particle's rotation over time, providing a measure of the rotational dynamics. The MSAD is given by

$$\langle \Delta\theta^2(\tau) \rangle = \langle [\theta(t + \tau) - \theta(t)]^2 \rangle_{\theta,t}, \tag{13}$$

where $\theta(t)$ represents the angular position of a particle at time t, and τ is the time lag (the difference between two time points). The averaging $\langle \cdot \rangle_{\theta,t}$ is performed over all particles and all times t. For a purely diffusive system, the MSAD is related to the rotational diffusion coefficient D_R as

$$\langle \Delta \theta^2(\tau) \rangle = 2dD_R\tau, \tag{14}$$

here, d is the number of dimensions in which the particle is free to rotate. This equation is linear, so by plotting $\langle \Delta \theta^2(\tau) \rangle$ versus τ, the rotational diffusion coefficient D_R can be determined from the gradient of the line divided by $2d$.

As $\langle \Delta \theta^2(\tau) \rangle$ is dimensionless and τ has units of time, D_R must have units of inverse time, the same units as the shear rate $\dot{\gamma}$. Thus, the Péclet number can be calculated as

$$\text{Pe} = \frac{\text{Vorticity}}{\text{Diffusion}} = \frac{\dot{\gamma}}{D_R}. \tag{15}$$

Determining the Péclet number is useful as it will allow us to determine how much noise we expect to see in the simulations, thus providing a measure of whether simulations are done correctly. This concludes our discussion on the fluid which the bananas are suspended in, we shall now move onto the bananas themselves.

2.3 Banana Definition

Before discussing the theoretical rotational trajectory of the banana, we provide a brief overview of how the banana is modelled and its key attributes. The internal mechanics (bonding and forces) are omitted for now, though they will be described in later sections. As mentioned earlier, in this project, we model bacteria as bananas. A banana is represented as a non-spherical rigid polymer consisting of six monomers. The curvature angle, θ, is defined as the angle between the centres of the first and last monomers, as illustrated in figure 2. The orientation angle, ϕ, is the angle between the $\hat{\boldsymbol{x}}$-direction and the principal component vector, $\boldsymbol{v}_p$. This unit vector, shown in blue in figure 2, indicates the direction of greatest variance within the banana and is always parallel with the vector connecting the centres of the first and final monomers.
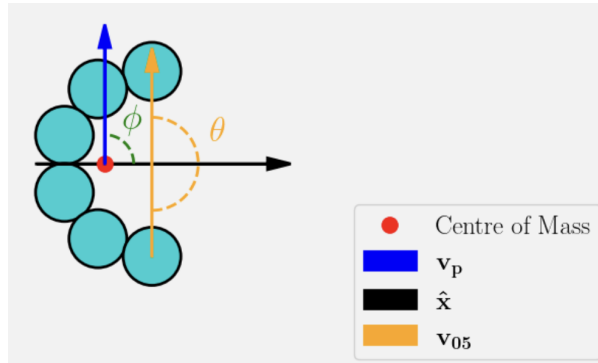

Figure 2: Representation of a banana, modelled as six monomers with curvature angle $\theta = \pi$ (orange). The vector connecting the centres of the first and final monomers is denoted $\boldsymbol{v}_{05}$ (orange). The centre of mass is marked in red, and the orientation angle ϕ (green) is the angle between the principal vector $\boldsymbol{v}_p$ and the $\hat{\boldsymbol{x}}$-direction.

The principal vector is important for two key reasons. First, it provides a straightforward method for tracking the orientation angle of the particle during the entire simulation.

Second, describing the rotational motion of the banana requires quantifying its shape, typically achieved using the aspect ratio, a dimensionless parameter that characterises an object's geometry [17]. Calculating the aspect ratio and determining the principal vector both involve eigenvalue decomposition. Thus, using the principal vector to track rotation not only simplifies the process but also reduces the computational workload.

To motivate this eigenvalue decomposition, we start by considering an ellipse in two dimensions. Here the aspect ratio simple to calculate by measuring the lengths of the major axis, a, and the minor axis, b, and taking their ratio

$$p = \frac{a}{b}. \tag{16}$$

Since bananas do not have clearly defined minor and major axes, a different method is required to calculate their aspect ratio: eigenvalue decomposition. To determine the aspect ratio, the gyration tensor [18] is computed. This tensor describes how much the monomers are spread out from a central point, in this case chosen to be the centre of mass

$$S_{mn} \overset{\text{def}}{=} \frac{1}{2N^2} \sum_{i=1}^{N} \sum_{j=1}^{N} (r_m^{(i)} - r_m^{(j)})(r_n^{(i)} - r_n^{(j)}), \tag{17}$$

where $r_m^{(i)}$ represents the m-th coordinate of the i-th monomer and N is the total number of monomers. The eigenvectors of this tensor represent the directions of principle variance within the banana. These vectors are denoted principal vector, $\boldsymbol{v}_p$ and minor vector, $\boldsymbol{v}_m$, corresponding to the directions of most and least variance respectively. The eigenvalues corresponding to these vectors are denoted λ_p and λ_m respectively, where $\lambda_p > \lambda_m$. Thus the ratio of these eigenvalues gives the aspect ratio

$$\mathrm{p} = \frac{\lambda_p}{\lambda_m}, \tag{18}$$

Theoretically, as the angle of curvature of the bananas is varied, this aspect ratio changes sharply tending to towards infinity as the curvature angle tends to one (figure 3).
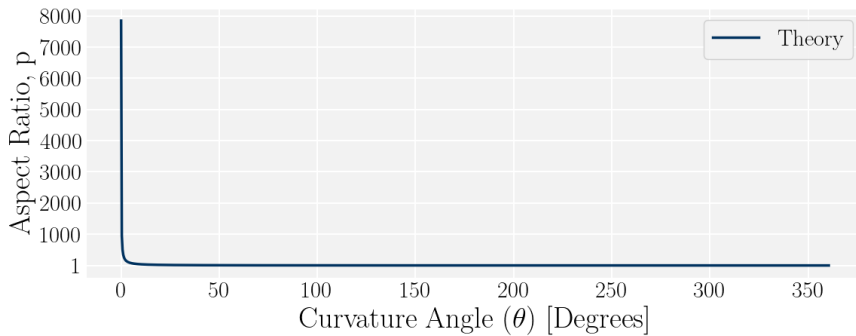

Figure 3: Aspect ratio as a function of the curvature angle. As the curvature angle approaches zero, the aspect ratio sharply tends to infinity, while as the curvature angle approaches 2π radians, the aspect ratio approaches 1.

7

With this aspect ratio, we are able to describe the theoretical rotational dynamics through Jeffery Orbits.

2.4 Jeffery Orbits

In the early 20th century, George B Jeffery completed a series of works that describes the trajectories of non-spherical particles suspended in fluid under the influence of a shear flow [19]. The most simple shapes are those with one axis of rotational symmetry, also known as axisymmetric shapes, such as ellipsoids or rods.

To describe the rotational trajectory of the banana. In the absence of any noise, in other words assuming rotation is solely due to vorticity. The rate of change of $\mathbf{v}_p$ with respects to time is given by [11]

$$\dot{\mathbf{v}}_p = \mathbf{v}_p \cdot \boldsymbol{\omega} + \frac{(p^2 - 1)}{p^2 + 1} \left(\mathbf{v}_p \cdot \mathbf{D} - \mathbf{v}_p \mathbf{v}_p \mathbf{v}_p : \mathbf{D} \right), \tag{19}$$

where p is the aspect ratio of the particle. Here, $\mathbf{D}$ and $\boldsymbol{\omega}$ are the strain rate and vorticity tensors, respectively. The symbol : denotes the double dot product.

In this equation, the term $\mathbf{v}_p \cdot \boldsymbol{\omega}$ represents the rotational motion of the particle solely due to vorticity, $\mathbf{v}_p \cdot \mathbf{D}$ corresponds to the strain in all directions and $\mathbf{v}_p \mathbf{v}_p \mathbf{v}_p : \mathbf{D}$ accounts for the strain parallel to the flow direction, thus leaving only the perpendicular strain component. If the parallel strain were included, it would elongate the object, which contradicts physical observations. The strain is scaled by a factor dependent on the aspect ratio p. In a two dimensional Couette flow, the tensors and orientation vector simplify to

$$\boldsymbol{\omega} = \begin{bmatrix} 0 & \frac{\dot{\gamma}}{2} & 0 \\ -\frac{\dot{\gamma}}{2} & 0 & 0 \\ 0 & 0 & 0 \end{bmatrix}, \quad \mathbf{D} = \begin{bmatrix} 0 & \frac{\dot{\gamma}}{2} & 0 \\ \frac{\dot{\gamma}}{2} & 0 & 0 \\ 0 & 0 & 0 \end{bmatrix}, \quad \mathbf{v}_p = \begin{bmatrix} \cos\phi \\ \sin\phi \\ 0 \end{bmatrix}. \tag{20}$$

Substituting these into equation 19 and integrating leads to an expression for the orientation angle, ϕ [20].

$$\tan\phi = p \tan\left(\frac{\dot{\gamma} t}{p + \frac{1}{p}} \right) + \tan\phi_0, \tag{21}$$

where $\dot{\gamma}$ is the shear rate and ϕ_0 is the initial orientation angle. This expression is differentiated to show how the orientation angle varies with time.

$$\dot{\phi} = \frac{d\phi}{dt} = \frac{p \frac{\dot{\gamma} t}{p + \frac{1}{p}} \sec^2\left(\frac{\dot{\gamma} t}{p + \frac{1}{p}} \right)}{1 + p^2 \tan^2\left(\frac{\dot{\gamma} t}{p + \frac{1}{p}} \right)}. \tag{22}$$

Here, ϕ is time-periodic and this rotation is called a Jeffery Orbit [19] with a period of

$$P = \frac{\pi}{\dot{\gamma}} \left(p + \frac{1}{p} \right). \tag{23}$$

As the aspect ratio approaches infinity, the period also approaches infinity. This behaviour is exemplified by the case of a thin, rigid rod: the rod rotates until its long axis aligns with the flow direction, at which point rotation ceases. For particles with a large but finite aspect ratio, rotation is slow when its principal vector (shown in figure 2) is parallel to the direction of flow and rapid when the principal vector is perpendicular to it. In the other limit, as the aspect ratio approaches zero, the time period also tends to infinity. This occurs with an infinitely flat and oblate particle, which similarly stops rotating once aligned with the flow direction. When the aspect ratio is exactly one, in two dimensions this situation arises with a circle, the time period is finite and given by

$$P = \frac{2\pi}{\dot{\gamma}}. \tag{24}$$

From the Jeffery orbit equations, the orientation angle can be calculated based on the aspect ratio. Specifically using equations 21 and 23 a preliminary analysis is conducted to visualise the orientation angle trajectory (figure 4), and angular velocity (figure 5), and the time period for all curvature angles, θ. In this analysis we assume rotation is solely due to vorticity no rotational diffusion (noise) is present.

The orientation angle trajectory has clear periodic motion (figure 4). As the principal vector rotates from parallel to perpendicular to the direction of fluid flow, the rate of this rotation varies significantly, for the 2π curvature it is constant however all others exhibit areas of accelerating and de-accelerating rotation. In all cases once perpendicular to the direction of fluid flow, the banana rapidly rotates $\frac{\pi}{2}$ radians so that the principal vector is parallel with the fluid once more.

As the curvature angle, increases from 0 to 2π radians, the time period decreases. The time taken for the principal axis to rotate from parallel to the shear flow to perpendicular increases. Although in all cases once the principal axis is orthogonal to the shear flow, the banana still rotates rapidly to be parallel with the fluid once more.
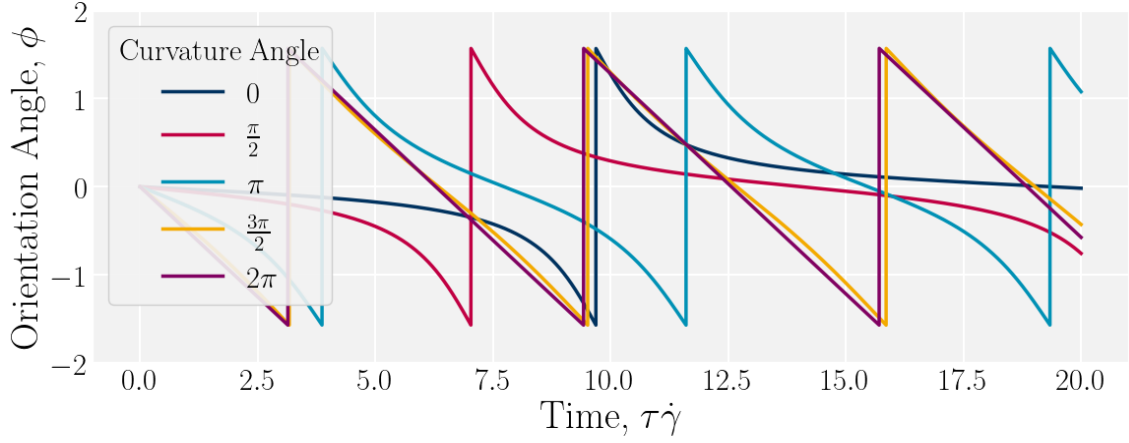
Figure 4: Theoretical expectation of the orientation angle, ϕ trajectory. Bananas with curvature angles varying from 0 to 2π radians are plot. Time is expressed in simulation units and multiplied by the shear rate $\dot{\gamma}$ to make dimensionless.

The angular velocity is at its lowest when the banana is aligned parallel to the fluid flow. As the banana rotates towards a perpendicular orientation, the angular velocity increases, reaching its maximum when the banana is perpendicular to the fluid flow. After reaching the peak, the angular velocity decreases again as the banana moves from the perpendicular orientation back to the parallel orientation, and this behaviour is repeated in a periodic fashion. As the curvature angle decreases from 2π to 0 radians, the rate of increase in angular velocity becomes more pronounced, resulting in a sharper peak, as shown in figure 5.
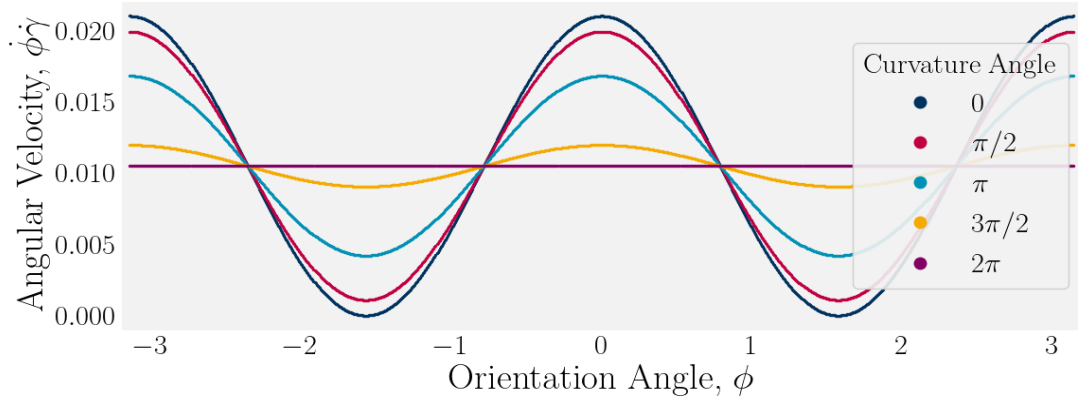

Figure 5: Theoretical expectation of the angular velocity, $\dot{\phi}$ as a function of the orientation angle, ϕ. Plotted for each banana with curvature angle varying from 0 to 2π radians. Angular velocity is multiplied by shear rate $\dot{\gamma}$ to make it dimensionless. The peaks correspond with the banana being perpendicular to the direction of flow and the troughs are where the banana is parallel to the direction of flow

This graphs provide the theoretical expectation of how the bananas will rotate and provide a useful benchmark for analysis later. In order to collect results, we move onto

the simulation mechanics.

3 Simulation Background

To run simulations Multi-Particle Collision Dynamics in Molecular Dynamics (MPCD in MD) is used. This method is selected because we are dealing with moderate Péclet numbers. In this section an overview of Multi-Particle Collision Dynamics (MPCD) and Molecular Dynamics (MD) schemes is given separately before explaining how these approaches are combined and the specific simulation setup for this project.

3.1 Multi-Particle Collision Dynamics

To investigate a banana's rotational behaviour in a fluid, Multi-Particle Collision Dynamics (MPCD) simulations are used simulate the fluid which a banana will be suspended in. MPCD was first proposed by Malevanets and Kapral [21]. It is a particle based method that simulates thermally fluctuating hydrodynamic interactions within fluids. MPCD is best for situations when both thermal fluctuations, small scale movements caused by thermal energy in the fluid and hydrodynamic interactions are crucial [22]. This corresponds to a moderate Péclet number.

MPCD is a coarse-grained, particle-based algorithm; It approximates solutions to the Navier-Stokes equations [23]. This approach does not model the interactions between individual particles at a microscopic level. Instead, it focuses on capturing the overall behaviour of the system on a coarser, mesoscopic scale, where the dynamics are represented by a set of mesoscopic particles that simulate the fluid's bulk properties. This means some molecular details are lost, nevertheless MPCD performs well on longer length and time scales. At each simulation step, momentum and energy are conserved within collisions, accurately representing hydrodynamics over extended time scales but becoming less reliable at microscopic scales [24]. MPCD treats the continuous fluid as a collection of point-like particles, which can be thought of as fluid of sand. This particle-based nature also enables a range of complex boundary conditions. In implementation, MPCD has two main steps: Streaming and collisions as shown in figure 6 [22].
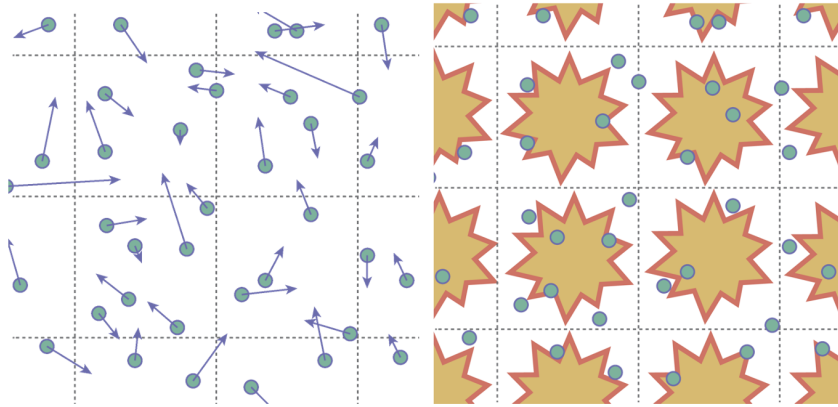

Figure 6: Illustrations of streaming (left) and collision (right) steps.

In the streaming step, particles, with velocity $\boldsymbol{v}_i$ and position $\boldsymbol{x}_i$ move freely based on their individual velocities. This step updates each particle's position without considering interactions with other particles. At this stage, if one was to discount the collisions step, the fluid would behave as an ideal gas. Each position is updated according to

$$\boldsymbol{x}_i(t + \delta t) = \boldsymbol{x}_i(t) + \boldsymbol{v}_i(t)\,\delta t, \tag{25}$$

where δt is the time-step interval, and i denotes the fluid particle.

Once streaming is completed, the system undergoes the collision step. Although there are multiple methods that can be utilised, each one is ultimately a non-physical scheme that conserves momentum [25]. Most schemes are designed so that the model recreates relevant transport coefficients and properties, such as viscosity and diffusivity. In this project, the chosen implementation scheme works by first grouping particles into cells. Within each cell the particles will collide locally exchanging particle properties, such as momentum via a stochastic collision operation [22]. Thus this step conserves momentum within each cell and introduces thermal fluctuations, hydrodynamic interactions and statistical noise.

At this stage, the MPCD algorithm is complete; however, modifications can be implemented to improve accuracy and capture additional information. A common enhancement addresses the loss of Galilean invariance, which arises due to the discretisation of the simulation domain into collision grid cells. Galilean invariance states that the laws of physics should remain the same in all inertial frames of reference. In MPCD, when the particle mean free path is smaller than the size of the collision cells, the discretisation can introduce artificial correlations in particle collisions. This happens because particles interact repeatedly with the same local neighbours, leading to unphysical behaviour [26]. To fix this issue, the collision cell grid is randomly shifted at each time-step (figure 7). Another common modification is to conserve angular momentum. From the collision, linear momentum is conserved but not angular momentum. In order to fix this one must trade energy conservation [27]. This adjustment may lead to small deviations in kinetic energy, which, if left unchecked, can cause fluctuations in the system's temperature. These temperature fluctuations could significantly affect the overall behaviour of the system, therefore a constant temperature must be maintained. To achieve this constant temperature in the system, the MPCD particles are coupled to a thermostat. Various thermostats, including Andersen's Thermostat [28] and Dissipative Particle Dynamics (DPD) [29], can be employed, though their detailed characteristics are not discussed here. In this project, both modifications are implemented: random grid shifting to ensure Galilean invariance and the Andersen Thermostat to maintain constant temperature.
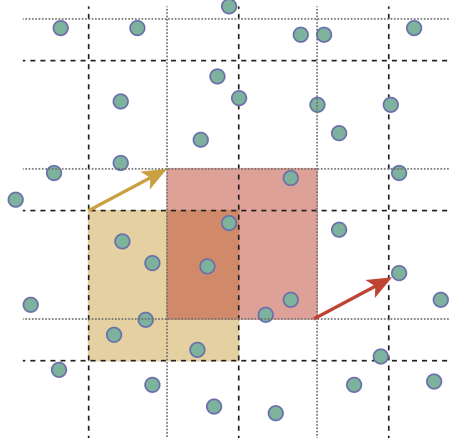
Figure 7: Illustration demonstrating how Galilean invariance is restored by randomly shifting the lattice of MPCD cells.

3.2 Molecular Dynamics

As previously mentioned, the bananas are treated as polymers which are comprised of a number of repeating units called monomers, which are connected and interact via bonds. A banana is simulated through Molecular Dynamics (MD); a common approach to simulate polymer dynamics as it follows the evolution of a large number of interacting particles [30].

In order to perform MD simulations, we must first consider the internal mechanics of the banana, i.e. the forces and potentials holding it together. To begin the net force on each particle is calculated through a series of pair potential schemes. One of the most common schemes is the Lennard-Jones (LJ) potential [23]. For two free, uncharged molecules (labelled i and j respectively), it is given by

$$U_{LJ}(r_{ij}) = 4\epsilon \left[\left(\frac{\sigma}{r_{ij}} \right)^{12} - \left(\frac{\sigma}{r_{ij}} \right)^{6} \right], \tag{26}$$

where, σ is the finite distance at which the inter-particle potential is zero, ϵ is the depth of the potential well, and r_{ij} is the distance between the two particles.

To isolate the repulsive interaction, the LJ potential is truncated and shifted at its minimum, $r_c = 2^{1/6}\sigma$, resulting in the Weeks-Chandler-Andersen (WCA) potential, as shown in figure 8. The WCA potential models excluded volume effects by enforcing a strong repulsion that prevents particles from overlapping at short distances [31]. This repulsive force is active up to r_c, ensuring that particles cannot get closer than this critical separation. Beyond r_c, the WCA potential is set to zero, meaning there are no interactions from WCA at larger distances, the WCA potential itself is given by

$$U_{\text{WCA}}(r_{ij}) = \begin{cases} 4\epsilon \left[\left(\frac{\sigma}{r_{ij}} \right)^{12} - \left(\frac{\sigma}{r_{ij}} \right)^{6} + \frac{1}{4} \right] & r_{ij} < r_c \\ 0 & r_{ij} > r_c \end{cases} \tag{27}$$

13

where $r_c = 2^{1/6}\sigma$.

In addition to the repulsive WCA interaction, we also include the Finitely Extensible Non-linear Elastic (FENE) potential [31]. The bond is modelled as a spring with a restoring force that gives rise to this potential, thus it connects the adjacent monomers to form the chain-like structure of the banana.

$$U_{\text{FENE}}(r_{ij}) = -\frac{k_{\text{FENE}}}{2} r_0^2 \ln\left(1 - \frac{r_{ij}^2}{r_0^2}\right), \tag{28}$$

where k_{FENE} is a spring constant representing the stiffness of the bond in response to stretching and r_0 is the equilibrium length of the bonds. These relationships are shown in figure 8.

The final potential we consider is the dihedral potential. This potential, $U_{\text{di}}(\theta)$, represents the energy associated with the torsional rotation around the bond between two monomers in the polymer chain [32], thus governing the rotational freedom of the bond. There are several forms of the dihedral potential, in these simulations, the harmonic form is used. Here the energy is minimised at a specific torsion angle ψ_0, and the potential increases quadratically with deviations from this angle, as shown in figure 8 and given by

$$U_{\text{di}}(\psi) = \frac{k_\psi}{2}(\psi - \psi_0)^2, \tag{29}$$

where k_ψ is the spring constant quantifying the stiffness of the dihedral angle potential. The angle ψ is the dihedral angle, which measures the relative rotation between two bond directions and ψ_0 is the equilibrium dihedral angle.
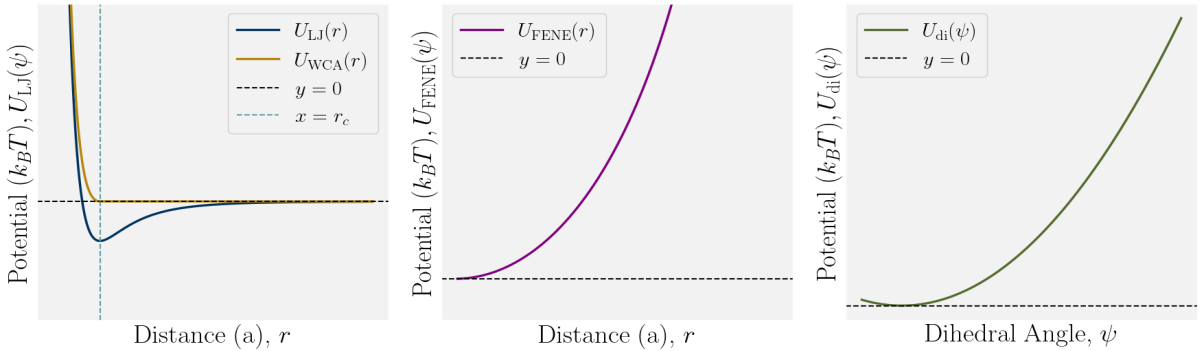

Figure 8: Potentials used to model interactions in the simulation. (Left) The Lennard-Jones (LJ) potential ($U_{LJ}(r)$, blue) considers both attractive and repulsive forces, while the WCA potential ($U_{WCA}(r)$, orange) is a purely repulsive truncated form of the LJ potential, with a cutoff at $r_c = 2^{1/6}\sigma$ (blue dashed line). (Middle) The FENE potential ($U_{FENE}(r)$, purple) displays bonded interactions with a steep rise near the maximum extension limit. (Right) The dihedral potential ($U_{di}(\psi)$, green) describes the rotational energy as a function of the torsional angle ψ. All quantities are expressed in simulation units, see section 3.5

Putting these potentials together, a polymer is modelled in a coarse-grained simulation as a freely joined chain of monomers, interacting by the WCA potential and bonded to

neighbouring monomers via the FENE and dihedral potentials. The overall force can be determined by taking the negative gradient of the potential.

$$\boldsymbol{F}_i = -\sum_j \nabla \left(U_{\mathrm{WCA}}(r_{ij}) \right) - \sum_j \nabla \left(U_{\mathrm{FENE}}(r_{ij}) \right) - \sum_j \nabla \left(U_{\mathrm{di}}(\psi_{ij}) \right). \tag{30}$$

Thus through Newton's second law the acceleration can be determined. With this acceleration, each time-step the position and velocity are updated through Verlet's algorithm

$$\boldsymbol{a}_i = \frac{\boldsymbol{F}_i}{m_i}, \tag{31}$$

$$\boldsymbol{v}_i \left(t + \frac{1}{2}\Delta t \right) = \boldsymbol{v}_i(t) + \frac{1}{2}\boldsymbol{a}_i(t)\Delta t, \tag{32}$$

$$\boldsymbol{x}_i(t + \Delta t) = \boldsymbol{x}_i(t) + \boldsymbol{v}_i \left(t + \frac{1}{2}\Delta t \right) \Delta t, \tag{33}$$

$$\boldsymbol{v}_i(t + \Delta t) = \boldsymbol{v}_i \left(t + \frac{1}{2}\Delta t \right) + \frac{1}{2}\boldsymbol{a}_i(t + \Delta t)\Delta t, \tag{34}$$

where $\boldsymbol{v}_i(t)$ and $\boldsymbol{x}_i(t)$ represent the velocity and position at time t, respectively; $\boldsymbol{a}_i(t)$ is the acceleration at time t, calculated from the forces acting on the particle; and Δt is the timestep size.

3.3 MD in MPCD

In summary, the fluid is modelled through MPCD and the bananas are modelled through MD. In order to collect data about bananas suspended in fluid, these methods are combined in the MD in MPCD scheme. This schemes works in the following manner, first the MPCD particles complete the streaming step. Next the MD algorithm updates the MD particles, (in our case one banana) trajectories over some defined number of MD time-steps, N_{MD} [22]. After this is complete, the MD particles are imported into the MPCD algorithm as a heavy particle and the collision step occurs. Both the MD particles and MPCD particles take part in the collision step. Then this cycle repeats and the MPCD particles (not the MD particles) complete streaming again and the MD algorithm is reinitiated for another N_{MD} MD time-steps, trajectory is updated then the MD particles are imported with the MPCD particles for the collision step. Including the MD particles in the collision step means that MD particles exchange momentum with the fluid [21].

3.4 Boundary Conditions

Although there are multiple boundary condition schemes, In this project, two are utilised, namely periodic boundary conditions and no-slip bounce back boundary conditions, shown in figure 9. First, periodic boundary conditions are where the banana and fluid particles will leave through one boundary, then enter through the opposite side. In order to achieve this, when the banana crosses the planar surface, it is offset by an

displacement equivalent to the length of the system [33]. Second, no-slip bounce back boundary conditions. These make all particles act like pool balls bouncing off the table's edge. With no-slip conditions, the tangential component of position is kept constant and the normal component is reversed.
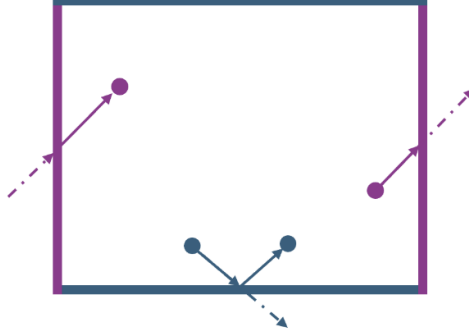

Figure 9: Schematic of simulation system, demonstrating the different boundary conditions The horizontal surfaces (blue) have no-slip bounce back boundary conditions, thus the particle bounces back the vertical walls (purple) have periodic boundary conditions, resulting in the particle leaving through one wall and entering through the other.

3.5 Units and Chosen Simulation Parameters

In this simulation, three quantities are defined as fundamental and are chosen to have a value of one. These are

- Mass, m - mass of a fluid particle.

- Length, a - defined as the cell size.

- Energy, $k_B T$ - thermal energy of the system, where k_B is the Boltzmann constant.

All other units are derived from these three fundamental units, For this project, significant ones are

$$\text{Velocity, } [v] = \beta = \sqrt{\frac{k_B T}{m}}, \tag{35}$$

$$\text{Time, } [t] = \zeta = a\sqrt{\frac{m}{k_B T}}. \tag{36}$$

In order to make certain quantities dimensionless, such as time and angular velocity, they are multiplied by the shear rate, $\dot{\gamma}$. Unless stated, all analysis is conducted in simulation units.

The simulations presented in this project are carried out in two dimensions with a system size of $30a \times 30a$ with boundary conditions as described in section 3.4. The MPCD particles are randomly initiated with positions from a uniform distribution and velocities

from the Maxwell Boltzmann distribution [34]. The MD particle (banana) is initialised at a random position and orientation. Each banana is initialised with the same parameters, except orientation angle. These extra parameters include the dihedral angle is set to zero and $K_{FENE} = 120.0$ in simulation units. This a considerable magnitude which is chosen because we want bananas to retain their shape throughout the entire simulation, in other words no deformation. In addition, the MD timestep is set as 0.002 with 50 MD timesteps for every MPCD timestep.

This completes the theory and setup of the simulations, however in order to run simulations we cannot directly input the shear rate. This is only changed via changing the wall speed of the top and bottom walls. Therefore the relationship between shear rate and wall speed must be calculated first.

3.6   Shear Rate

To briefly revisit our overall motivation, rotation in sludge systems occurs due to both vorticity and diffusion (although dominated by vorticity), making a moderate Péclet number an appropriate model for this system. This is further justified by the fact that, given our use of MPCD for these simulations, a high Péclet number is not possible. Since we are interested in rotation dominated by vorticity, a low Péclet number is undesirable. Therefore, a moderate Péclet number is preferred. To achieve this, we examine the relationship between shear rate and wall speed.

First the relationship between average flow speed and flow height is determined with a wall speed of 1β. To calculate this, multiple MPCD simulations (no MD inclusion) are run with 10000 timesteps and a 10000 step warmup. The relationship between these quantities is determined to be $v_x = 0.00141y - 0.02025$ (figure 10). This has a low chi-square value ($\chi^2 = 0.10822$), signifying good agreement and a tight fit to the trendline, The high number of simulation steps and warm-up steps contribute to the tight fit. The shear rate for Couette flow is given by the gradient of the trendline, thus this is found to be $0.00141\zeta^{-1}$. The flow speed jumps at two points, $y = 0a$ and $y = 30a$, this corresponds to the flow at the horizontal walls therefore these points are discounted from analysis.
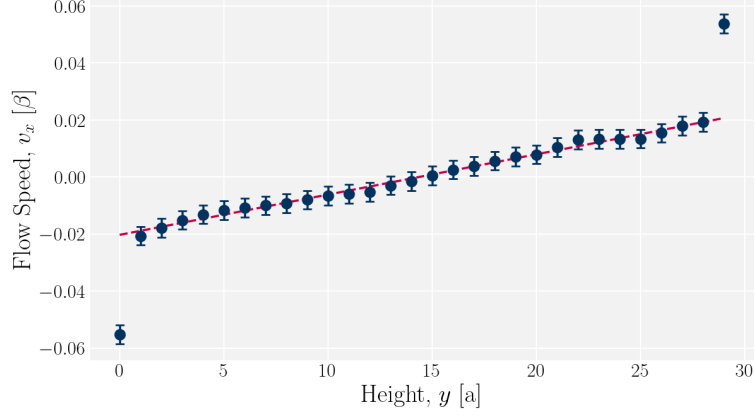
Figure 10: Relationship between flow height, y and average flow speed, v_x. The trendline is given by $v_x = 0.00141y - 0.02025$, with a chi-squared statistic, $\chi^2 = 0.10822$, demonstrating a tight fit to the trendline. The shear rate is calculated to be $0.00141\zeta^{-1}$.

Although this is useful to gauge what the shear flow is for an exact wall speed, in order to run simulations one requires a direct relation between wall speed and shear rate. To determine this, 14 simulations are conducted with wall speeds ranging from 0.1β to 10β. This results in a trendline of $\dot{\gamma} = 0.0027v_x - 0.00001$ (figure 11). The agreement between the data and the trendline is evaluated using the chi-squared statistic, which is calculated to be 0.01199, indicating excellent agreement.
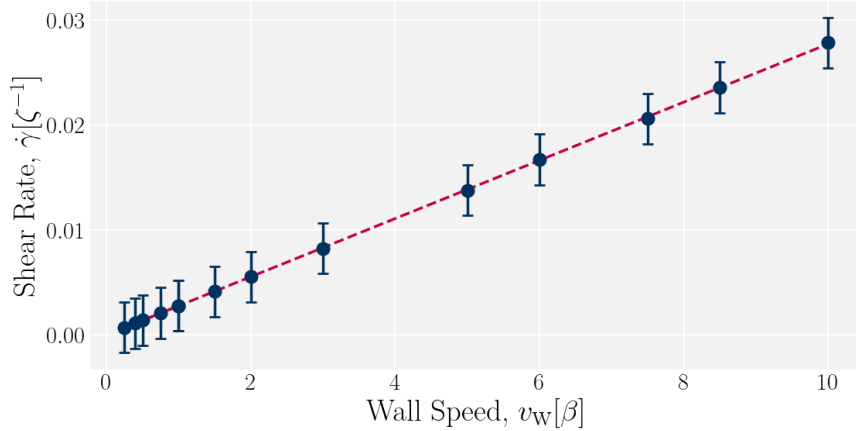
Figure 11: Linear relationship between wall speed, v_w and shear rate, $\dot{\gamma}$. Each point represents a simulation at a specific wall speed. The fitted trendline is $\dot{\gamma} = 0.0027v_w - 0.00001$, with a chi-squared statistic of 0.01199.

As stated earlier we require a moderate Péclet number so that vorticity is dominating the rotational dynamics. To determine what shear rate this corresponds to, multiple simulations with a rod-banana (curvature angle 0) and different wall speeds are run. These simulations are visually analysed to assess whether sufficient rotation occurred, ensuring the motion was not dominated by rotational diffusion (noise). It is concluded that a wall speed of 8β achieves this. From figure 11, one can see this corresponds to

a shear rate of $0.022\zeta^{-1}$. All simulations are conducted using this wall speed unless specified otherwise. This concludes the simulation setup.

4   Results

Simulations are performed for curvature angles of 0, $\frac{\pi}{2}$, π, $\frac{3\pi}{2}$, and 2π radians. Prior to data collection, the MPCD fluid undergoes a warm-up phase of 2000 MPCD timesteps, during which the banana remains stationary. Simulations are run for 5×10^6 timesteps, corresponding to an approximate runtime of five hours, unless otherwise stated. This duration was agreed to be appropriate as to collect a sufficient amount of data. During the simulation, data is recorded for monomer positions and the centre of mass. The collected data is subsequently analysed and animated using a series of Python scripts. The simulations and data analysis is repeated to check reproducibility and ensure outcomes are consistent.

Analysis begins by looking at the centre of mass trajectory, aspect ratio and principal vector. These results serve as tests to ensure simulations are running correctly and these quantities have been calculated correctly. Then we proceed to look at rotational dynamics, comparing results with theory presented in section 2.3. First to understand the simulations, representative snapshots from the animation for each banana are shown in figure 12.
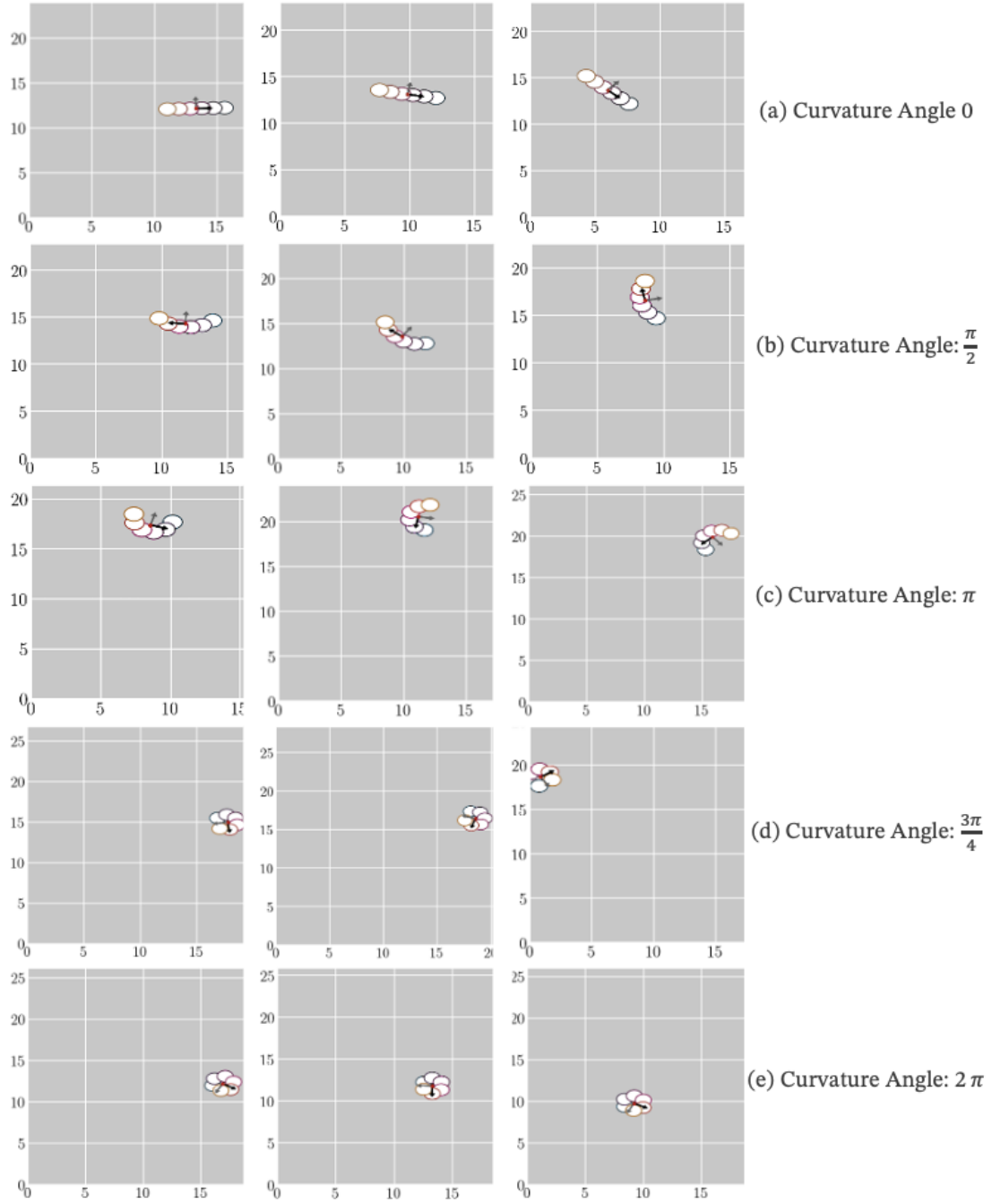
Figure 12: Series of snapshots for bananas with curvature angles of 0, $\frac{\pi}{2}$, π, $\frac{3\pi}{2}$, and 2π radians. Each series of snapshots are taken 10 timesteps apart with the centre of mass (red circle), principal vector, $\boldsymbol{v}_p$ (black), and minor vector, $\boldsymbol{v}_m$ (grey).

4.1 Centre of Mass Trajectory

Solely looking at a banana with a $\frac{\pi}{2}$ curvature angle, the x-trajectory reflects the periodic boundary conditions, while the y-trajectory demonstrates random motion with an upward trend. As the particle moves upward towards the wall, its speed increases, as evidenced by the increasing frequency in the x-plot, reflecting the Couette shear profile. This is shown in figure 13. Similar stochastic behaviour is shown by other curvature angles although omitted here due to space concerns.
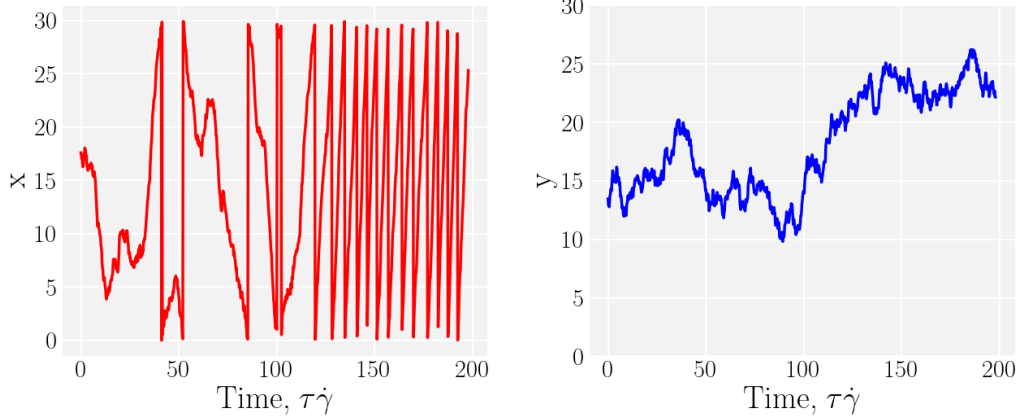
Figure 13: Temporal evolution of the bananas' centre of mass. The bananas has curvature angle $\frac{\pi}{2}$. The x trajectory (left) showcases periodic behaviour due to boundary conditions and the y trajectory (right) displays a stochastic upward drift upwards.

4.2 Aspect Ratio and Principal Vector

In order to calculate the orientation angle and angular velocity, first the principal vector and aspect ratio must be determined by the process described in section 2.3. To begin the aspect ratio is calculated and shown to follow the same trend as the theoretical prediction in figure 3, this is displayed in figure 14. As the curvature angle tends to 2π the aspect ratio tends to one and there is a significant increase for a curvature angle of zero.
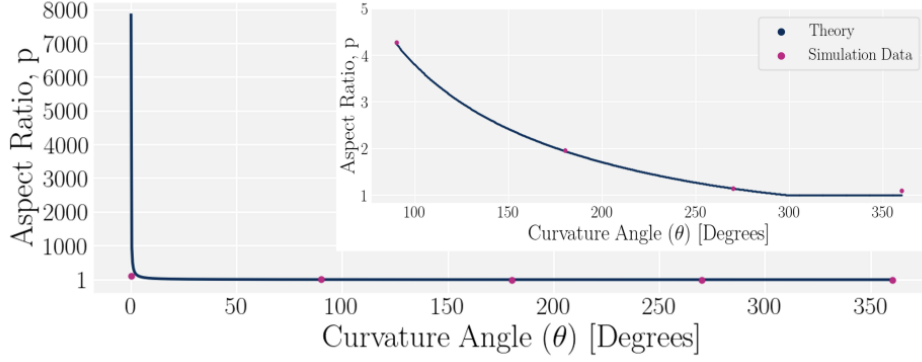
21

Figure 14: Relationship between aspect ratio and curvature angle. As the curvature angle approaches zero, the aspect ratio tends to infinity, while as the curvature angle approaches 2π radians, the aspect ratio approaches one. The smaller insert shows this with 0 curvature omitted. Both graphs are plotted with theory data in blue and simulation data in pink.

Overall there is good agreement with theoretical aspect ratios, however there are deviations for curvature angles of 0 and 2π. The 0 curvature angle can be explained as the rod, in practise, is not an infinitely thin rod, which leads to a smaller aspect ratio than predicted. In the case of the circle, the theoretical aspect ratio of the circle should be 1.00 however through the simulation the average aspect ratio is calculated as 1.10. This likely arises from simulation implementation, the bonds between monomers are not rigid enough thus it is possible a higher value of K_{FENE} may prevent this. Although further work would be required to confirm this.

Next the principal vector, $\boldsymbol{v}_p$ is calculated. Here we focus on the banana with curvature angle of $\frac{\pi}{2}$. To ensure it is correctly orientated throughout the entire simulation, the dot is product with the vector connecting the first monomer to the final monomer, $\boldsymbol{v}_{05}$ is plot (figure 15). As both vectors are normalised and the result is one for the duration of the simulation, demonstrating they are always parallel to each other, thus ensuring the correct orientation angle is always calculated when looking at the rotational dynamics. All other curvatures show the same behaviour therefore are omitted due to space concerns.
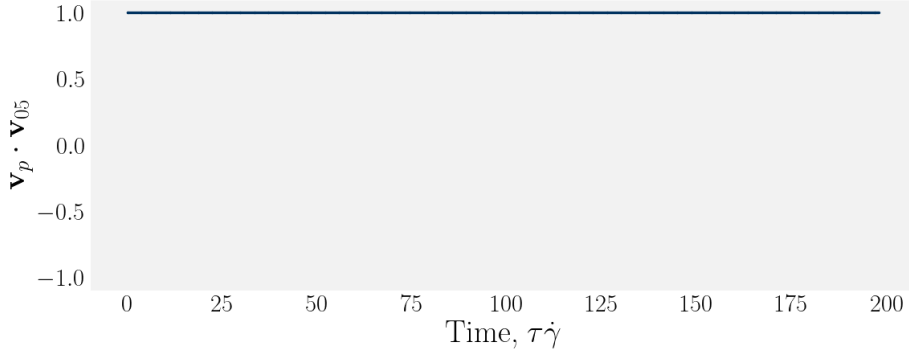
Figure 15: The dot product between the principal vector, $\boldsymbol{v}_p$ and vector from first to final monomer, $\boldsymbol{v}_{05}$ for a banana with a curvature angle of $\frac{\pi}{2}$ radians. Both vectors are normalised and their dot product is consistently one.

4.3   Rotational Dynamics

To begin, we look at the orientation angle trajectory. Using the principal vector, the orientation angle was calculated through the inverse tangent function. This trajectory (figure 16), despite the high volume of noise, shows an evolution over time that matches the theoretical shape (figure 4), albeit with an irregular period caused by diffusive motion (noise). Across all curvature angles, the trajectory exhibits rapid rotation when transitioning from an orthogonal orientation to parallel with the flow ($\phi = 0$ to $\phi = \pm\frac{\pi}{2}$) and slower rotation when moving from parallel to orthogonal orientation ($\phi = \pm\frac{\pi}{2}$ to $\phi = 0$).

Next the angular velocity is considered. This differentiation was conducted through a five point stencil [35] to mitigate some of the noise and sharp peaks seen in figure 4. Despite this mitigation, the angular velocity plots (figures 17, 18) also display a high level of noise, in order to see the long term motion clearer, the angular velocity is plot against the unwrapped orientation angle (figure 17). This demonstrates clear clusters of data, the frequency of these clusters decreases as the angle of curvature increases.

The theoretical expectations are calculated based on the average aspect ratio from the simulation and utilising mathematics explain in section 2.4. These are plot with the wrapped data (figure 18). Although difficult to see peaks, there are clear clusters slightly right of the theoretical peaks. To further demonstrate the pattern in the wrapped data, the data was binned across the orientation angle and averaged over the angular velocity (figure 18). These binned plots better demonstrate the curved trajectories expected from the theoretical predictions, although there are still clear deviations from the theory, suggesting that diffusive rotation is playing a significant role still.
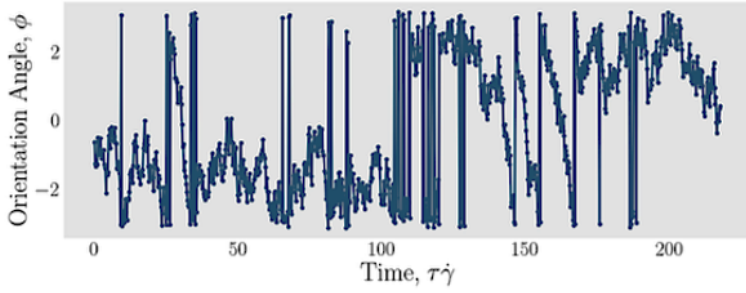
To test the fit of the data, residuals for the wrapped angular velocity are plot (figure 19), these show a linear trend for small curvature angles and clustering at the edges of the domain, indicating a poor fit to the data however this fit improves for higher curvature angles.
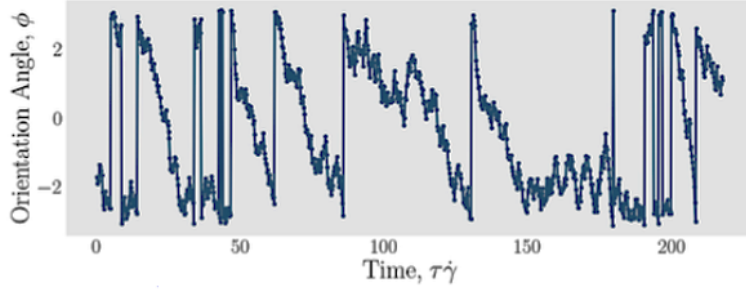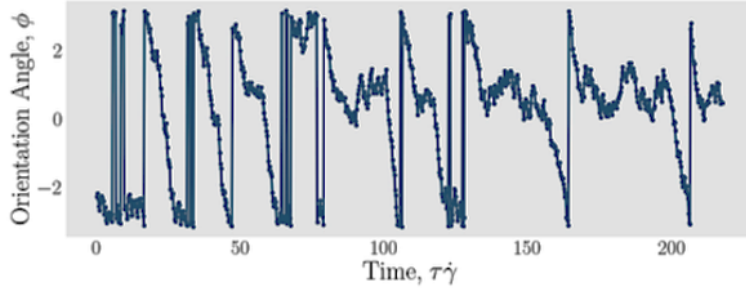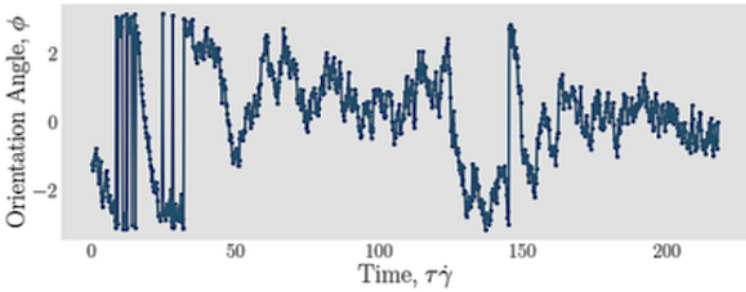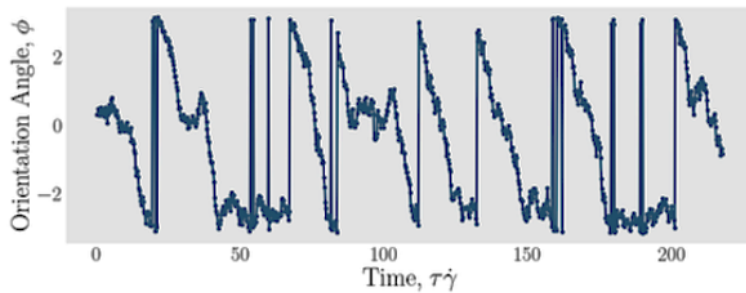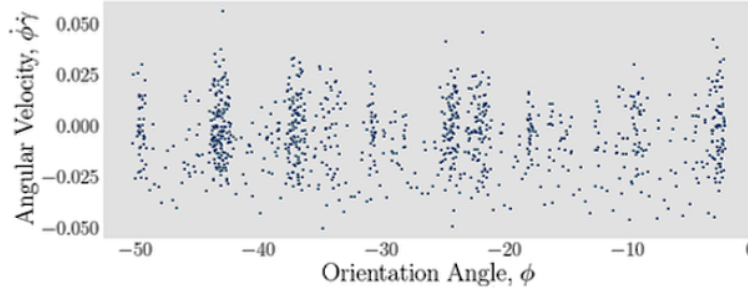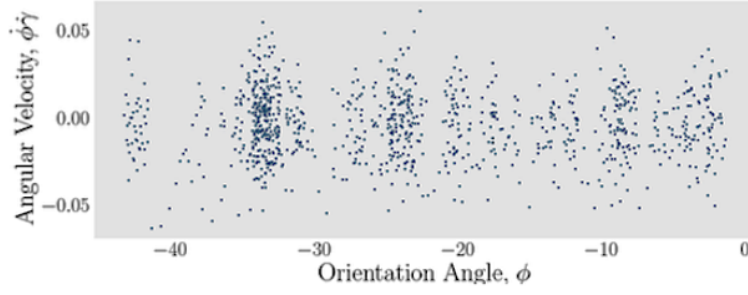
23

Figure 16: Evolution of the banana's orientation with time. Rows correspond to increasing curvature values: 0 (top), $\frac{\pi}{2}$, π, $\frac{3\pi}{2}$, and 2π (bottom).
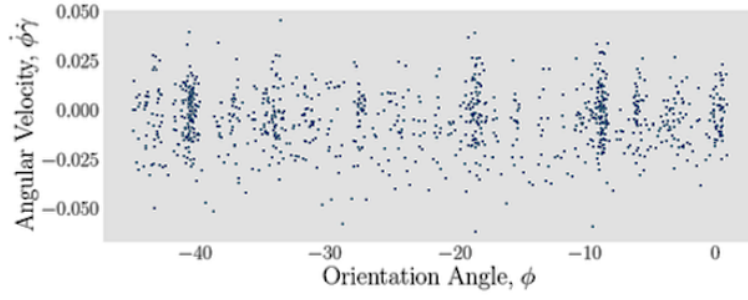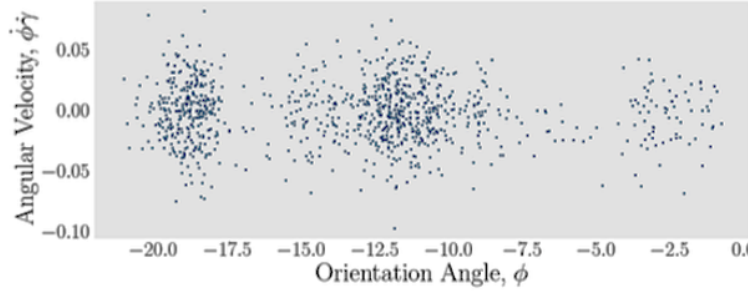
Figure 17: Comparison of angular velocity as a function of the unwrapped orientation angle for different curvatures. Rows correspond to increasing curvature values: 0 (top), $\frac{\pi}{2}$, π, $\frac{3\pi}{2}$, and 2π (bottom). The unwrapped data demonstrates data clusters an irregular time period of rotation with frequency that decreases as the angle of curvature increases
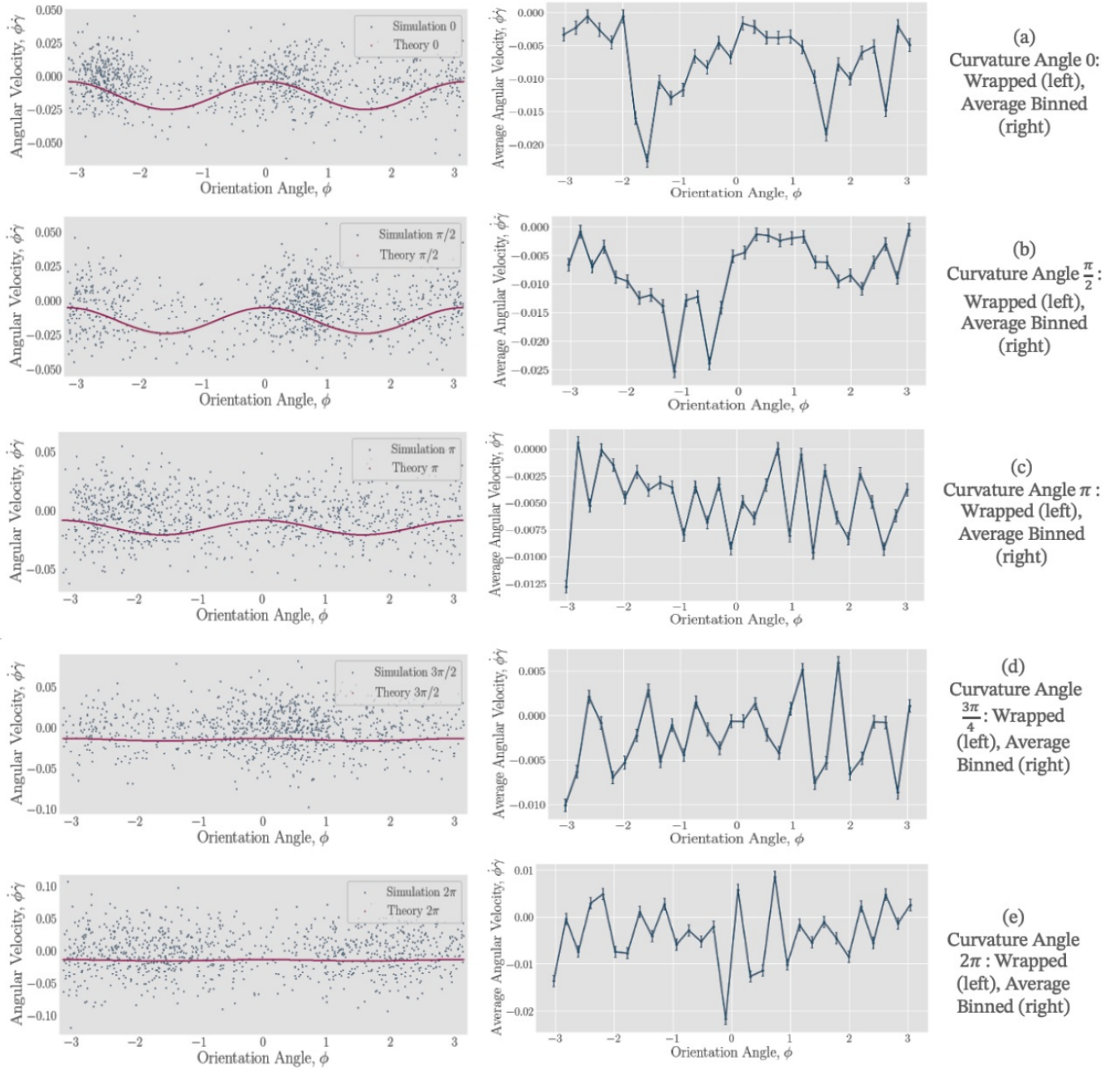
Figure 18: Comparison of angular velocity as a function of orientation angle for different curvatures. The first column overlays the wrapped simulation data with the theoretical predictions (pink curve), while the second column shows data binned across orientation angle and averaged over the angular velocity. Rows correspond to increasing curvature values: 0 (top), $\frac{\pi}{2}$, π, $\frac{3\pi}{2}$, and 2π (bottom). The first column demonstrate clustering in line with theoretical predictions which is clearer in the second column.

Figure 19: Residual values from theoretical model against the corresponding theoretical angular velocities. Top left: 0 curvature, top right: $\frac{\pi}{2}$, middle left: π, middle right: $\frac{3\pi}{4}$ and bottom: 2π. Error bars calculated from standard deviation. Residuals demonstrate a linear trend for low curvature angles
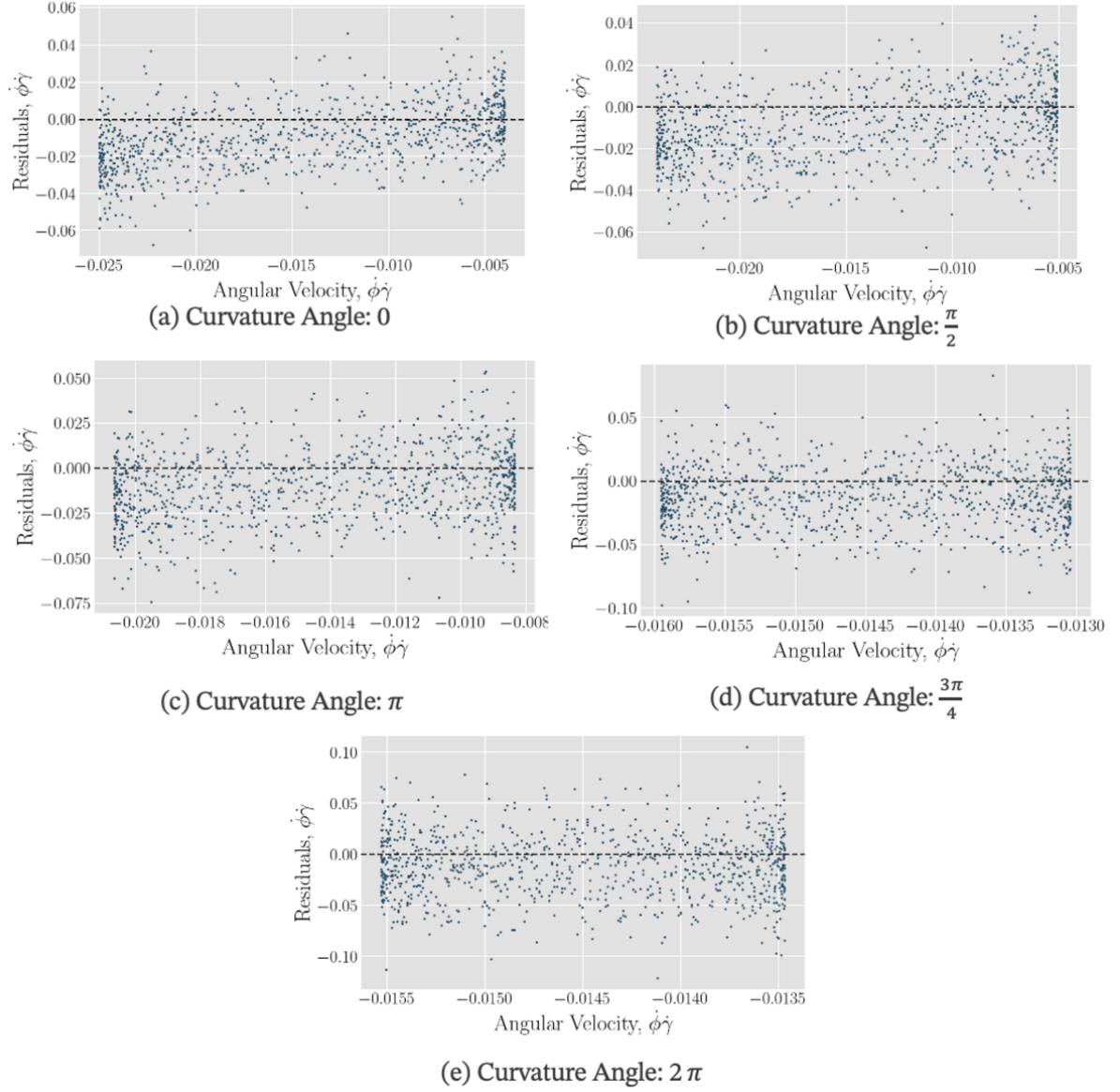
4.4   Péclet Number

Throughout analysis it is highly likely that the diffusive rotation (noise) is still playing a considerable role in addition to rotation caused by vorticity. Therefore to confirm this and better understand the level of noise we expect from the system, the Péclet number is calculated specifically for the rod banana (0 curvature). A long simulation (5×10^8 timesteps) is performed with no wall speed, thus zero shear flow so rotation is solely diffusive. To calculate the MSAD, the rod is split into three pairs of molecules (dimers), then the MSAD is calculated for each pair. This is plotted against the lagtime, as shown

27

in figure 20. The linear section of the graph at small lagtimes corresponds to rotation due to diffusion. By applying curve fitting to this linear section and following the method explain in section 2.2, a diffusion constant, D_R is obtained to be 0.00170 ± 0.00001. From here, by dividing the shear rate by the diffusion coefficient, the Péclet number is calculated to be 12.91 ± 0.59. Since this value is greater than one, it indicates that vorticity dominates the flow; however, being only one order of magnitude higher than unity, we would expect diffusive rotation to remain significant. As seen through the rotational dynamics graphs.
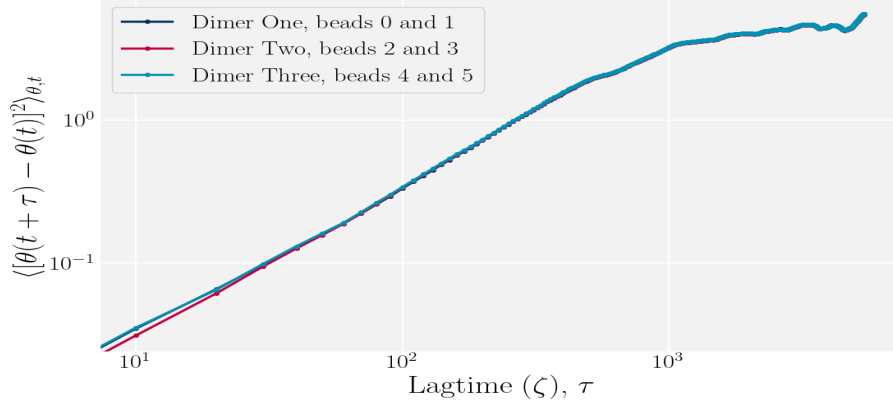

Figure 20: Mean Square Angular Displacement as a function of Lagtime for each dimer. Dimers exhibit the highly similar trajectories; They display a linear trend for short lagtimes which is characteristic of diffusive motion.

5   Discussion

To begin, the orientation angle trajectory (figure 16) demonstrates that while the period of rotation is irregular due to noise; as the curvature angle increases the rotation period decreases. This effect can be explained solely through noise. Considering the rod (banana with zero curvature), it will rotate parallel to the shear flow and remain in this configuration indefinitely as there is no upward or downward force acting upon it. Adding noise to the system introduces random perturbations that displace the rod either upwards or downwards, thereby inducing a random walk like behaviour that can increase the rate of rotation. The likelihood of increasing the rate of rotation is probabilistic and could be tied to the Péclet number; further studies are needed to confirm this. This phenomenon is also observed for other curvature angles, though it becomes less pronounced as curvature angle increases to the point where it has very little effect for a circle, due to its symmetry. This effect is reflected throughout angular velocity graphs (figure 18 and figure 17) through the high volume of data rightwards of the theoretical peak, where the banana is transitioning from being parallel to the fluid to an orthogonal orientation.

Looking in further detail at the angular trajectory (figure 18). From the theory, the theoretical aspect ratio of the circle should be 1.00 however through the simulation the average aspect ratio is calculated as 1.10; implying that the monomers of the banana

28

are not always touching and there is a noticeable degree of internal movement. This movement is reflected through the clustering of data in figure 17. If the aspect ratio was exactly one, it is expected that data is uniformly distributed however this does not occur. This likely occurs due to either simulation artifacts or the value of K_{FENE} is too small, although further study is necessary to confirm this.

The residuals plot (figure 19) shows a clear linear trend for rods, which weakens as the curvature angle increases. Focusing on the rod, this linear trend corresponds to the trough-to-peak transition, indicating that deviations from the model are greatest at these points. The clustering pattern observed earlier is also present here. As the curvature angle increases, the residuals become more randomly distributed, suggesting a better fit to the theoretical model. This improvement likely results from the isotropic shape of circular particles, where noise acts uniformly in all directions. By contrast, rods are more sensitive to the direction of noise; perturbations parallel the rod's major axis have less impact compared to those acting perpendicular to it.

Up to this point, it is clear that noise plays a considerable role in the rotational dynamics, a role far bigger than curvature. The expected level of noise is quantified through the Péclet number (12.91 ± 0.59). The figure is one order of magnitude greater than unity, thus noise is expected to play a significant role in the bananas rotation despite not being primary driver of rotation. To achieve cleaner results, one could repeat the analysis with a system with a higher Péclet number. This could be achieved by increasing the wall speed which would increase the shear rate. However this approach may increase the chance of banana disintegration at the horizontal walls. As the walls move, a banana hitting the wall experiences a significant force that exceeds the attractive forces binding the monomers together, as observed at wall speeds of 8β. Overall, systems with higher Péclet numbers are not ideal for two main reasons: first, MPCD is effective only for moderate Péclet numbers, meaning an alternative simulation method without noise would be required. Second, moderate Péclet numbers reflect real-world sludge bulking systems, where noise is always present.

6 Conclusion

Overall it is found that although curvature impacts the rotational dynamics of banana-shaped colloids (bananas), the effects of noise overshadow those from curvature. This conclusion is reached by studying the dynamics of five bananas with curvature angles of 0, $\frac{\pi}{2}$, π, $\frac{3\pi}{4}$, and 2π. These bananas were simulated using a Molecular Dynamics in Multi-Particle Collision Dynamics (MD in MPCD) approach. Each banana was suspended in a box with constant fluid with shear rate $0.022\zeta^{-1}$. The box consisted of two vertical walls with periodic boundary conditions and two horizontal walls with bounce back boundary conditions. The centre of mass of each particle displayed random motion in both the x- and y-directions due to thermal fluctuations, with periodic boundary conditions in x. To determine the orientation angle and angular velocity, the principal vector and aspect ratio were determined through eigenvector decomposition of the gyration tensor, which were shown to be consistently parallel with the orientation vector of the particle.

The orientation angle and angular velocity trajectories show that the rotation period increases as the curvature angle increases. Furthermore results demonstrate high levels of irregularities in the time period. Both of these effects were explained through noise. This high level of noise introduced significant deviations from the theoretical model although clusters of data were observed to be slightly rightwards of the theoretical peaks, implying a degree of agreement with Jeffery orbit theory, which was better observed through binning the data.

The residual plots demonstrated a linear trend in residuals for low curvature angles indicating a poor fit to the theoretical model. The ratio of vorticity to diffusion was given by the Péclet number of 12.91 ± 0.59. Thus providing evidence that diffusive rotation (noise) plays a critical role in these simulations despite vorticity being the dominant mode of transport. Thus it is clear we can conclude that noise impacts the rotational dynamics far more than curvature.

For sludge bulking applications, these results show that noise plays a more significant role in rotational dynamics than the curvature of a single banana with a moderate Péclet number. However, in a multi-banana system, curvature could influence interactions, potentially causing bananas to hook together and form more complex shapes, which would significantly affect rotation. Therefore, curvature cannot be entirely discarded in these systems.

Future work could explore a-thermal simulations, which would remove noise and provide further evidence that the bananas follow a Jeffery orbit trajectory and how curvature affects rotational dynamics. However, for sludge bulking applications, this may not be highly useful, as real systems always involve some degree of thermal fluctuations or noise. Therefore, studying the hydrodynamic and mechanical interactions between multiple bananas suspended in a fluid could be more beneficial, as it would enhance our understanding of bacteria movement and how they clump together to cause sludge bulking.

References

[1] A. Creppy et al. "Effect of Motility on the Transport of Bacteria Populations Through a Porous Medium". In: *Phys. Rev. Fluids* 4 (1 Jan. 2019), p. 013102. DOI: 10.1103/PhysRevFluids.4.013102. URL: https://link.aps.org/doi/10.1103/PhysRevFluids.4.013102.

[2] S. Rossetti et al. "*Microthrix parvicella*, a Filamentous Bacterium Causing Bulking and Foaming in Activated Sludge Systems: A Review of Current Knowledge". In: *FEMS Microbiology Reviews* 29.1 (Jan. 2005), pp. 49–64. ISSN: 0168-6445. DOI: 10.1016/j.femsre.2004.09.005. eprint: https://academic.oup.com/femsre/article-pdf/29/1/49/18127280/29-1-49.pdf. URL: https://doi.org/10.1016/j.femsre.2004.09.005.

[3] P. H. Nielsen et al. "Identity and ecophysiology of filamentous bacteria in activated sludge". In: *FEMS Microbiology Reviews* 33.6 (Nov. 2009), pp. 969–998. ISSN: 0168-6445. DOI: 10.1111/j.1574-6976.2009.00186.x. eprint: https://academic.oup.com/femsre/article-pdf/33/6/969/18142178/33-6-969.pdf. URL: https://doi.org/10.1111/j.1574-6976.2009.00186.x.

[4] A. M. P. Martins et al. "Filamentous Bulking Sludge — A Critical Review". In: *Water Research* 38.4 (2004), pp. 793–817. ISSN: 0043-1354. DOI: https://doi.org/10.1016/j.watres.2003.11.005. URL: https://www.sciencedirect.com/science/article/pii/S004313540300616X.

[5] W. Burger et al. "The Influence of Protruding Filamentous Bacteria on Floc Stability and Solid-Liquid Separation in the Activated Sludge Process". In: *Water Research* 123 (2017), pp. 578–585. ISSN: 0043-1354. DOI: https://doi.org/10.1016/j.watres.2017.06.063. URL: https://www.sciencedirect.com/science/article/pii/S0043135417305390.

[6] J.-A. Ulbrich et al. "Effect of Curvature on the Diffusion of Colloidal Bananas". In: *Phys. Rev. E* 107 (4 Apr. 2023), p. L042602. DOI: 10.1103/PhysRevE.107.L042602. URL: https://link.aps.org/doi/10.1103/PhysRevE.107.L042602.

[7] J. W. Garvin. *A Student's Guide to the Navier-Stokes Equations*. Cambridge: Cambridge University Press, Sept. 2023, p. 224. ISBN: 9781009236164.

[8] M. O. Deville. *An Introduction to the Mechanics of Incompressible Fluids*. Cham, Switzerland: Springer Nature Switzerland AG, 2022. ISBN: 978-3-031-04682-7. DOI: 10.1007/978-3-031-04683-4. URL: https://doi.org/10.1007/978-3-031-04683-4.

[9] D. Pnueli and C. Gutfinger. "Exact Solutions of the Navier-Stokes Equations". In: *Fluid Mechanics*. Cambridge University Press, 1992, pp. 179–212.

[10] B. E. Rapp. "Chapter 9 - Fluids". In: *Microfluidics: Modelling, Mechanics and Mathematics*. Ed. by Bastian E. Rapp. Micro and Nano Technologies. Oxford: Elsevier, 2017, pp. 243–263. ISBN: 978-1-4557-3141-1. DOI: https://doi.org/10.1016/B978-1-4557-3141-1.50009-5. URL: https://www.sciencedirect.com/science/article/pii/B9781455731411500095.

[11] R. G. Larson. *The Structure and Rheology of Complex Fluids*. Topics in Chemical Engineering. New York, Oxford: Oxford University Press, 1999. ISBN: 0-19-512197-X.

[12] A. P. Philipse. *Brownian Motion: Elements of Colloid Dynamics for Nano-Materials Science*. Undergraduate Lecture Notes in Physics. Cham, Switzerland: Springer Nature Switzerland AG, 2018. ISBN: 978-3-319-98052-2. DOI: `10.1007/978-3-319-98053-9`. URL: `https://doi.org/10.1007/978-3-319-98053-9`.

[13] A. J. Majda and A. L. Bertozzi. *Vorticity and Incompressible Flow*. Cambridge Texts in Applied Mathematics. Cambridge University Press, 2001.

[14] F. P. Incropera and D. P. DeWitt. *Introduction to Heat Transfer*. Wiley, 1985. ISBN: 9780471801269. URL: `https://books.google.co.uk/books?id=f9hAAQAAIAAJ`.

[15] J. X. J. Zhang and K. Hoshino. "Chapter 3 - Microfluidics and Micro Total Analytical Systems". In: *Molecular Sensors and Nanodevices (Second Edition)*. Ed. by J. X. J. Zhang and K. Hoshino. Second. Academic Press, 2019, pp. 113–179. ISBN: 978-0-12-814862-4. DOI: `https://doi.org/10.1016/B978-0-12-814862-4.00003-X`. URL: `https://www.sciencedirect.com/science/article/pii/B9780128148624000003X`.

[16] J. P. Segovia-Gutiérrez et al. "Diffusion of Anisotropic Particles in Random Energy Landscapes—An Experimental Study". In: *Frontiers in Physics* 7 (2020). DOI: `10.3389/fphy.2019.00224`. URL: `https://doi.org/10.3389/fphy.2019.00224`.

[17] B. E. Rapp. "Chapter 9 - Fluids". In: *Microfluidics: Modelling, Mechanics and Mathematics*. Ed. by B. E. Rapp. Micro and Nano Technologies. Oxford: Elsevier, 2017, pp. 243–263. ISBN: 978-1-4557-3141-1. DOI: `https://doi.org/10.1016/B978-1-4557-3141-1.50009-5`. URL: `https://www.sciencedirect.com/science/article/pii/B9781455731411500095`.

[18] H. Arkın and W. Janke. "Gyration Tensor Based Analysis of the Shapes of Polymer Chains in an Attractive Spherical Cage". In: *The Journal of Chemical Physics* 138.5 (2013), p. 054904. ISSN: 0021-9606. DOI: `10.1063/1.4788616`. URL: `https://doi.org/10.1063/1.4788616`.

[19] G. B. Jeffery. "The Motion of Elliptical Particles Immersed in a Viscous Fluid". In: *Proceedings of the Royal Society of London. Series A, Containing Papers of a Mathematical and Physical Character* 102.715 (1922), pp. 161–179. DOI: `10.1098/rspa.1922.0078`. URL: `https://doi.org/10.1098/rspa.1922.0078`.

[20] S. A. Abtahi and G. J. Elfring. "Jeffery Orbits in Shear-Thinning Fluids". In: *Physics of Fluids* 31.10 (2019). Submitted: 23 August 2019; Accepted: 6 October 2019; Published Online: 24 October 2019, p. 103106. DOI: `10.1063/1.5125468`. URL: `https://doi.org/10.1063/1.5125468`.

[21] S. A. Rice, ed. *Advances in Chemical Physics*. Vol. 140. Advances in Chemical Physics. Hoboken, New Jersey: John Wiley & Sons, Inc., 2008. ISBN: 978-0-470-22688-9.

[22] M. P. Howard, A. Nikoubashman, and J. C. Palmer. "Modeling Hydrodynamic Interactions in Soft Materials with Multiparticle Collision Dynamics". In: *Current Opinion in Chemical Engineering* 23 (2019). Frontiers of Chemical Engineering: Molecular Modeling, pp. 34–43. ISSN: 2211-3398. DOI: `https://doi.org/10.1016/j.coche.2019.02.007`. URL: `https://www.sciencedirect.com/science/article/pii/S2211339819300024`.

[23] C. Holm and K. Kremer. *Advanced Computer Simulation Approaches for Soft Matter Sciences III*. Ed. by Christian Holm and Kurt Kremer. 1st ed. Vol. 221. Advances in Polymer Science. Springer Berlin Heidelberg, 2009, pp. xiv, 237. ISBN: 978-3-540-87705-9. DOI: `10.1007/978-3-540-87706-6`. URL: `https://doi.org/10.1007/978-3-540-87706-6`.

[24] C. M. Pooley and J. M. Yeomans. "Kinetic Theory Derivation of the Transport Coefficients of Stochastic Rotation Dynamics". In: *The Journal of Physical Chemistry B* 109.13 (2005), pp. 6505–6513. DOI: `10.1021/jp046040x`. URL: `https://doi.org/10.1021/jp046040x`.

[25] R. G. Winkler et al. "Simulation of Complex Fluids by Multi-Particle-Collision Dynamics". In: *Computer Physics Communications* 169.1 (2005). Proceedings of the Europhysics Conference on Computational Physics 2004, pp. 326–330. ISSN: 0010-4655. DOI: `https://doi.org/10.1016/j.cpc.2005.03.073`. URL: `https://www.sciencedirect.com/science/article/pii/S0010465505001700`.

[26] T. Ihle and D. M. Kroll. "Stochastic Rotation Dynamics. I. Formalism, Galilean invariance, and Green-Kubo Relations". In: *Phys. Rev. E* 67 (6 June 2003), p. 066705. DOI: `10.1103/PhysRevE.67.066705`. URL: `https://link.aps.org/doi/10.1103/PhysRevE.67.066705`.

[27] H. Noguchi, N. Kikuchi, and G. Gompper. "Particle-Based Mesoscale Hydrodynamic Techniques". In: *Europhysics Letters* 78.1 (Mar. 2007), p. 10005. DOI: `10.1209/0295-5075/78/10005`. URL: `https://dx.doi.org/10.1209/0295-5075/78/10005`.

[28] P. J. Hoogerbrugge and J. M. V. A. Koelman. "Simulating Microscopic Hydrodynamic Phenomena with Dissipative Particle Dynamics". In: *Europhysics Letters* 19.3 (June 1992), p. 155. DOI: `10.1209/0295-5075/19/3/001`. URL: `https://dx.doi.org/10.1209/0295-5075/19/3/001`.

[29] H. C. Andersen. "Molecular Dynamics Simulations at Constant Pressure and/or Temperature". In: *The Journal of Chemical Physics* 72.4 (Feb. 1980), pp. 2384–2393. ISSN: 0021-9606. DOI: `10.1063/1.439486`. eprint: `https://pubs.aip.org/aip/jcp/article-pdf/72/4/2384/18920903/2384\_1\_online.pdf`. URL: `https://doi.org/10.1063/1.439486`.

[30] G. W. Slater et al. "Modeling the Separation of Macromolecules: A Review of Current Computer Simulation Methods". In: *Electrophoresis* 30.5 (2009), pp. 792–818. DOI: `https://doi.org/10.1002/elps.200800673`. eprint: `https://analyticalsciencejournals.onlinelibrary.wiley.com/doi/pdf/10.1002/elps.200800673`. URL: `https://analyticalsciencejournals.onlinelibrary.wiley.com/doi/abs/10.1002/elps.200800673`.

[31] T.-H. Wu and D. Qi. "Advantages of a Finite Extensible Nonlinear Elastic Potential in Lattice Boltzmann Simulations". In: *The Hilltop Review* 7.1 (2014). URL: https://scholarworks.wmich.edu/hilltopreview/vol7/iss1/10.

[32] M. Bulacu et al. "Improved Angle Potentials for Coarse-Grained Molecular Dynamics Simulations". In: *Journal of Chemical Theory and Computation* 9.8 (2013), pp. 3282–3292. DOI: 10.1021/ct400219n. eprint: https://doi.org/10.1021/ct400219n. URL: https://doi.org/10.1021/ct400219n.

[33] J. K. Whitmer and E. Luijten. "Fluid–Solid Boundary Conditions for Multiparticle Collision Dynamics". In: *Journal of Physics: Condensed Matter* 22.10 (Feb. 2010), p. 104106. DOI: 10.1088/0953-8984/22/10/104106. URL: https://dx.doi.org/10.1088/0953-8984/22/10/104106.

[34] S. J. Blundell and K. M. Blundell. "The Maxwell-Boltzmann distribution". In: *Concepts in Thermal Physics*. Oxford University Press, Oct. 2009. ISBN: 9780199562091. DOI: 10.1093/acprof:oso/9780199562091.003.0005. eprint: https://academic.oup.com/book/0/chapter/194777504/chapter-pdf/47109379/acprof-9780199562091-chapter-5.pdf. URL: https://doi.org/10.1093/acprof:oso/9780199562091.003.0005.

[35] C. R. Taylor. *Finite Difference Coefficients Calculator*. https://web.media.mit.edu/~crtaylor/calculator.html. Accessed: 2024-11-23. 2016.